Space Weather

RESEARCH ARTICLE
10.1029/2023SW003852

Effects of Forbush Decreases on the Global Electric Circuit

J. Tacza[1,2,3], G. Li[4,5], and J.-P. Raulin[3]

[1]Institute of Geophysics, Polish Academic of Sciences, Warsaw, Poland, [2]HUN-REN Institute of Earth Physics and Space Science, Sopron, Hungary, [3]Center of Radio Astronomy and Astrophysics Mackenzie, Engineering School, Mackenzie Presbyterian University, Sao Paulo, Brazil, [4]CSPAR, University of Alabama in Huntsville, Huntsville, AL, USA, [5]Department of Space Science, University of Alabama in Huntsville, Huntsville, AL, USA

Key Points:

- Measurement of cosmic rays by the AMS-02 experiment can be used to classify FD events as an alternative to the traditional NM measurements
- PG in fair weather conditions is shown to increase for large FD events but not for small FD events
- The Dst and Kp indices are shown to correlate with PG for large FD events but not for small FD events

Correspondence to:
G. Li,
gangli.uah@gmail.com

Citation:
Tacza, J., Li, G., & Raulin, J.-P. (2024). Effects of Forbush Decreases on the global electric circuit. *Space Weather*, *22*, e2023SW003852. https://doi.org/10.1029/2023SW003852

Received 30 DEC 2023
Accepted 4 MAR 2024

Abstract The suppression of high-energy cosmic rays, known as Forbush decreases (FDs), represents a promising factor in influencing the global electric circuit (GEC) system. Researchers have delved into these effects by examining variations, often disruptive, of the potential gradient (PG) in ground-based measurements taken in fair weather regions. In this paper, we aim to investigate deviations observed in the diurnal curve of the PG, as compared to the mean values derived from fair weather conditions, during both mild and strong Forbush decreases. Unlike the traditional classification of FDs, which are based on ground level neutron monitor data, we classify FDs using measurements of the Alpha Magnetic Spectrometer (AMS-02) on the International Space Station. To conduct our analysis, we employ the superposed epoch method, focusing on PGs collected between January 2010 and December 2019 at a specific station situated at a low latitude and high altitude: the Complejo Astronómico El Leoncito (CASLEO) in Argentina (31.78°S, 2,550 m above sea level). Our findings reveal that for events associated with FDs having flux amplitude (A) decrease $\leq$10%, no significant change in the PG is observed. However, for FDs with $A > 10\%$, a clear increase in the PG is seen. For these $A > 10\%$ events, we also find a good correlation between the variation of Dst and Kp indices and the variation of PG.

Plain Language Summary The Earth's atmosphere is constantly bombarded by highly energetic charged particles originating from the Sun, our own Milky Way galaxy, as well as from distant galaxies. These energetic charged particles penetrate Earth's magnetosphere and ionosphere and continually interact with the Earth's atmosphere, and these interactions have a significant impact on our environment. In the context of our research, we are specifically interested in a phenomenon known as Forbush Decreases. These occurrences involve the temporary suppression of the flow of energetic charged particles. Our study focuses on understanding how Forbush Decreases influence Earth's electrical activity, particularly in relation to the atmospheric electric field, also known as the potential gradient. To do this, we have gathered data from a high-altitude station situated at ~2.5 kms from the sea level. Our research findings have revealed that the potential gradient in the atmosphere is exceptionally responsive to strong Forbush Decreases. In simpler terms, when these suppression events take place, they have a noticeable and distinctive effect on the electrical characteristics of Earth's atmosphere, which we measure as changes in the potential gradient.

1. Introduction

The global electric circuit (GEC) is a complex system that connects the Earth's surface with the lower atmosphere (Haldoupis et al., 2017). This circuit involves various processes, including charge separation in disturbed weather regions and current flows in fair weather regions. In disturbed weather regions, thunderstorms occur and they are often referred to as "electric batteries." These storms give rise to ascending vertical currents, moving from the tops of thunderclouds to the lower boundary of the ionosphere. In contrast, in fair weather regions, there are descending vertical currents, moving from the atmosphere to the ground. To complete the electric circuit, there are currents that flow in two directions: (a) from fair weather to disturbed weather regions through the Earth's surface, which includes both lands and oceans, and (b) from disturbed weather to fair weather regions through the upper boundary of the circuit (Rycroft et al., 2008). The driving forces behind the GEC primarily include thunderstorms and electrified rain/shower clouds (Liu et al., 2010; Wilson, 1921). In addition to these atmospheric phenomena, the GEC can be influenced by high energetic charged particles from space. This influence is more pronounced at high latitudes (Rycroft et al., 2012). This is because charged particles penetrate more easily the polar region of the Earth's magnetic field. The GEC model supports the existence of an atmospheric electric field in fair weather regions (low wind speed, low cloud cover, no hydrometeors), caused by thunderstorms and electric shower clouds occurring in disturbed weather. This atmospheric electric field has a diurnal variation and is known as the

Carnegie curve after being discovered by the Carnegie Institute in the last century when multiple measurements over the oceans were performed (Harrison, 2013). Measurements of the atmospheric electric field on land can be disturbed by local effects such as natural radioactivity, convective processes in the planetary boundary layer, and pollution among others (Nicoll et al., 2019). However, when these local effects are correctly identified it is possible to study the impact of global effects (Tacza et al., 2020).

Cosmic rays consist of predominantly high-energy charged particles, such as protons and atomic nuclei, as well as a smaller fraction of neutral particles, including neutrons and neutrinos, and photons, all with energies significantly higher than the average energy of thermal particles in Earth's background plasma. They originate from various sources, including extragalactic cosmic rays with energies reaching up to 10^{21} eV, galactic cosmic rays (GCRs) up to 10^{16} eV, and solar cosmic rays with energies up to $15 - 30$ GeV/nuc (Dorman, 2004). Upon entering the Earth's atmosphere, cosmic rays interact with atmospheric particles, leading to the production of secondary particles, including neutrons. These neutrons can then be detected by neutron monitors (NMs) installed around the world (A global neutron monitor database (NMDB) can be found at https://www.nmdb.eu/). It is known that solar disturbances can induce variations in cosmic ray flux. A typical example of such variation is the phenomenon known as Forbush decrease (FD), characterized by sudden depressions in the cosmic ray flux (Cane, 2000). FDs can be caused by both the more regular 27-day solar rotation cycle (Simpson, 1954) and the transient Coronal Mass Ejections (CMEs). In both cases, variations of solar wind plasma parameters, including magnetic field and density, hinders the propagation of high energy cosmic rays near the Earth, leading to the decrease of cosmic ray flux. In the cases where the FDs are caused by solar rotations, Co-Rotating Interaction Regions (CIRs) are often involved (Guo & Florinski, 2014). CIRs can lead to stronger solar wind turbulence and affect particle diffusion coefficients. This will affect the GCR flux at 1 au, in a similar fashion as the seed populations in large SEP events (Wijsen et al., 2023).

Classification of FDs is traditionally through NM data (Usoskin et al., 2008). NMs measure the flux of high-energy neutrons on the Earth's surface. Because these neutrons are secondary cosmic rays, which are produced when primary cosmic rays, typically protons or atomic nuclei, interact with the Earth's atmosphere, their fluxes correlate with that of the primary cosmic rays. However, because the cascading process is complicated and because the energy resolution of neutron monitors are very coarse, to obtain the corresponding decrease profiles of the primary cosmic rays from NM data during FDs is very hard. In recent years, a number of space-born detectors have obtained direct measurements of primary cosmic-ray spectra in space. Wang et al. (2023) used daily proton data, measured by the Alpha Magnetic Spectrometer (AMS-02) on the International Space Station, to study the rigidity dependence of a large number of FD events. Alania and Wawrzynczak (2008) had earlier examined possible rigidity dependence of FDs. They assumed that the flux variation, dF in a FD event, normalized by the pre-event flux F_0, is proportional to the particle rigidity to a power of γ, that is, $dF/F_0 \sim R^{-\gamma}$. They showed that during the course of the 6–20 November 2004 FD event, a clear correlation between the intensity decrease and the power law index γ existed. They extend these to more events in a later work (Alania & Wawrzynczak, 2012). However, Wang et al. (2023) found that in many FD events, an exponential functional form fits better than a power law for the rigidity dependence. The Amplitude decrease we used in this work is based on the work of Wang et al. (2023). The period of study was from 2011 to 2019. Direct measurements of primary GCRs from ∼1 GeV/nuc to above 10 GeV/nuc are obtained. Because these measurements are made at an orbit altitude of ≥300 km, correlating these measurements with NM data around the globe can help to understand the underlying physical cascading processes (e.g., the production rate of secondaries) of cosmic rays in the atmosphere and the resulting measurements of PG (including its latitudinal and altitude dependence).

Several early studies have analyzed the FD effects on the GEC. These studies have focused on the disturbed and fair weather regions with inconclusive results. In disturbed weather regions, using the World Wide Lightning Location Network (WWLLN) data, Okike (2019) found a regional reduction in the lightning occurrence rate after 4 days of the FD onset (18% in the USA latitude band and 9% in Africa). Okike and Umahi (2019) also found a global lightning reduction of 3% on the same day of the FD onset. Due to the high day-to-day variation of the GEC, Okike and Umahi (2019) used the Superposed Epoch Analysis (SEA). The SEA is a statistical method used to analyze time series data in order to identify common patterns or trends across multiple events (Chree, 1913). The method involves aligning the events of interest to a common reference point (e.g., the onset of the event), and then averaging the data across all events to create a composite waveform. This composite waveform represents the average behavior of the system during the events of interest. Okike and Umahi (2019) defined the FD onset as the time when the cosmic rays reduction is maximum. In another two studies, applying

the SEA to the lightning data from the Lightning Imaging Sensor (LIS) on board the Tropical Rainfall Measuring Mission (TRMM) Satellite from 1998 to 2014, Wu et al. (2019) and Zhang et al. (2020) found a lightning activity decrease of 65% and 10%, respectively, after 3 days of the FDs onset. In these studies, the FD onset was defined as the start of the decrease of the cosmic ray flux. The percentile difference between these two studies could be due to the number of FDs analyzed. Wu et al. (2019) analyzed 28 FD and Zhang et al. (2020) 70 FDs.

In fair weather regions, Sheftel et al. (1994) used several mid-latitude stations and found an immediate increase in the current density following the onset of six FD events, after applying the SEA. Here, the FD onset was defined as the time of the maximum depression in the cosmic ray flux. In another study, Engfer and Tinsley (1999) examined PG variation recorded at Mauna Loa (3,400 m asl) in association with FD events using the SEA (FD onset was defined as the start of the decrease of the cosmic ray flux). The authors analyzed 93 FDs and found a 8.5% PG increase 4 days after the FD onset, however, the results were not significant. In yet another study, Marcz (1997), upon examining data recorded at the Nagycenk Observatory (Hungary, altitude: 154 m asl) during 60 FD events, the author found, after applying the SEA, a 5% PG decrease 2 days after the FD onset. However, the author pointed out that the results depended of the timing of the FD onset. Recently, Tacza et al. (2022) examined FDs with magnitude greater than 4% as recorded by the IZMIRAN database and did not find any significant PG variations, as recorded at the CASLEO observatory (18 events, high altitude station) and at the SWIDER observatory (15 events, low altitude station). The authors also defined the FD onset as the start of the cosmic rays flux decrease. However, individual analysis for very strong FDs (magnitude greater than 7%) showed a PG increase at CASLEO observatory. Clearly, there are disagreements on the PG effect of the FDs by these previous studies. These disagreements could be due to the timing of the FD onset (i.e., start time of the decrease in the cosmic rays flux or the time when the cosmic ray flux decrease was maximum), the number of FD events analyzed, and the magnitude of the FDs selected in the studies.

The magnitude of FDs is quantified by the parameter "MagnM", derived from a world-wide network of neutron monitors, specifically for 10 GV rigidity particles (Belov et al., 2005, 2018). The "MagnM" value is calculated using the Global Survey Method (GSM), a comprehensive technique developed by Belov et al. (2018). This method combines worldwide neutron monitor data, incorporating corrections for geomagnetic and atmospheric disturbances, device-specific characteristics, and various cosmic ray anisotropies. It employs a sophisticated spherical analysis to deduce the galactic cosmic ray density and anisotropy, facilitating an accurate estimation of cosmic ray flux variations outside the Earth's atmosphere and magnetosphere, with hourly precision (Belov et al., 2018). Moreover, GSM's refinement for magnetospheric effects accounts for how geomagnetic disturbances modify the effective cutoff threshold rigidity and the asymptotic directions of incoming primary particles across various neutron monitor stations. This adjustment is pivotal for the accurate assessment of cosmic ray variations, ensuring that the GSM's outputs reflect changes in cosmic ray intensity with a high degree of precision. Nevertheless this method is based on secondary neutrons measured at the ground to infer the flux of primary cosmic rays for specific events. It therefore can cause uncertainty and ambiguity of the classification of FDs. This ambiguity can be partially removed if one uses data of primary cosmic rays from, for example, the AMS-02 measurement onboard ISS, as done in Wang et al. (2023). In this work, we examine how the variations of primary cosmic ray intensity affects the GEC by using the amplitude reduction parameter proposed and computed in Wang et al. (2023). Our current work is an extension of the analysis presented in Tacza et al. (2022) and uses potential gradient data recorded between January 2010 and December 2019 at a high-altitude station in Complejo Astronómico El Leoncito.

Our paper is organized as the follows. In Section 2, the observation site and methodology are described. In Section 3, we present the results. Finally, we discuss and summarize our results in Section 4.

2. Site Location and Methodology

The CASLEO observatory is a place for observing astronomical phenomena located in an area known as "El Leoncito." This area has over 250 clear-sky days per year, with almost no wind and a clear, pollution-free atmosphere. The nearest town, Barreal, is located 40 km away. To measure the atmospheric electric field, a BOLTEK field mill sensor is used, which records PG values (PG = −Ez, where Ez is the vertical atmospheric electric field). The sensor is mounted on a steel support 0.4 m above the surface. The PG values are reduced to the value at free flat area at ground level and 1-s averages of the PG are processed.

Table 1
List of Forbush Decreases Events Examined in This Study

Event	FD onset Date—Time (UT)	FD max decrease Date—Time (UT)	IZMIRAN MagnM (%)	AMS-02 A (%)	Source Activity
1	2011.06.22—03:00	2011.06.24—00:00	4.1	8.3	CIR
2	2011.08.05—17:51	2011.08.05—21:00	4.8	13.6	ICME
3	2011.09.26—12:35	2011.09.27—00:00	5.1	19.3	ICME
4	2011.10.24—18:31	2011.10.25—00:00	6.5	10.3	ICME
5	2012.06.16—20:19	2012.06.18—00:00	4.0	12.8	ICME
6	2012.07.14—18:09	2012.07.15—15:00	7.6	19.4	ICME
7	2012.11.12—23:11	2012.11.13—15:00	4.1	6.7	ICME
8	2012.11.23—21:51	2012.11.25—00:00	3.6	6.9	ICME
9	2013.03.17—05:59	2013.03.19—00:00	4.3	14.1	ICME
10	2013.04.13—22:54	2013.04.15—00:00	4.4	7.9	ICME
11	2013.06.23—04:26	2013.06.24—00:00	5.3	4.1	CIR
12	2014.02.27—16:50	2014.02.28—15:00	4.9	10.0	CIR
13	2014.04.18—02:00	2014.04.20—00:00	3.0	9.6	ICME
14	2014.06.07—16:52	2014.06.08—00:00	3.9	NA[a]	ICME
15	2014.12.21—19:11	2014.12.22—18:00	6.0	16.9	ICME
16	2015.03.17—04:45	2015.03.18—00:00	5.6	12.7	ICME
17	2015.06.22—18:33	2015.06.23—00:00	9.1	15.2	ICME
18	2015.08.25—23:00	2015.08.26—03:00	3.5	5.9	ICME
19	2015.11.06—18:18	2015.11.07—02:00	3.1	3.5	ICME
20	2017.07.16—05:59	2017.07.16—18:00	5.8	14.2	ICME

[a]We treat this event as $A \leq 10$ when performing the SEA.

The term "fair-weather conditions" refers to weather conditions with little or no cloudiness, no precipitation, fog or dust, and no strong wind speed at the measurement site. Previous research has shown that reliable PG diurnal variations can be obtained under fair-weather conditions at CASLEO (Tacza et al., 2021). To ensure that fair-weather conditions are met at CASLEO, a Cloud Sensor II (Boltwood Systems Corporation) and a Vantage Pro (Davis Instruments) are used to monitor cloudiness and other meteorological parameters such as precipitation, wind speed (<6 m/s), and relative humidity (<90%). Harrison and Nicoll (2018) have proposed that a relative humidity of <95% (and visibility of 2–5 km or greater) is necessary to fulfill the criterion of lack of hydrometeors using automated measurements.

We correlate the PG data with FD measurements examined in Wang et al. (2023). Recently Wang et al. (2023) examined FDs using AMS-02 observations onboard ISS. Unlike previous studies that using neutron monitor data on the Earth's surface, the study of Wang et al. (2023) used daily proton flux data from the AMS-02 instrument to identify and classify 142 FD events between May 2011 and October 2019. Since the orbit of ISS is at an altitude of ∼370–460 km, the FDs observed in Wang et al. (2023) are in the ionosphere. One might expect that the global electric circuit is less affected by conditions up high in the ionosphere, however, as our analyses below show, there is a clear correlation between PG and large amplitude FDs observed by AMS-02.

Upon examination we find 20 FDs reported in Wang et al. (2023) had fair weather conditions at the CASLEO station. These FDs are shown in Table 1. The first column of Table 1 is event number. The second and third columns show the FD onset and maximum decrease times. The fourth column is the magnitude of the decrease (in percentage) provided by the IZMIRAN catalog (http://spaceweather.izmiran.ru/eng/dbs.html). The fifth column is the FD Amplitude A. This value is obtained by fitting the normalized FD amplitude rigidity spectrum with an exponential form as (Wang et al., 2023),

$$\Phi_{norm} = C - a * e^{-\alpha R} \quad (1)$$

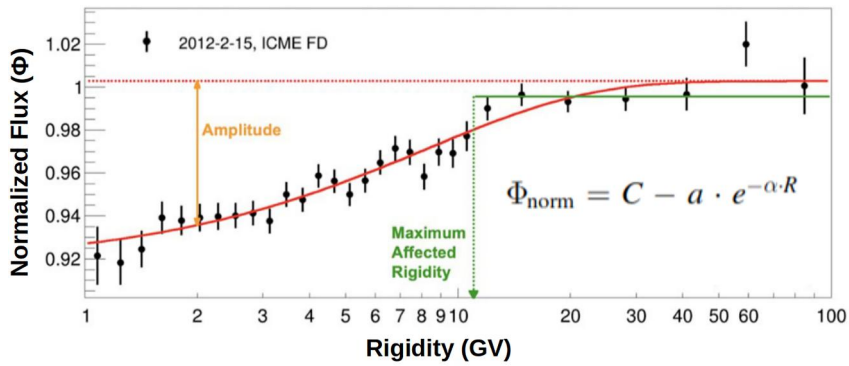

Figure 1. Amplitude parameter A used in this work. Data points with uncertainty bars are the daily Rigidity spectrum for a FD on 15 February 2012 (the minimum flux day), normalized to the reference spectrum on 13 February 2021, the day before the onset of the ICME on 14 February 2021. The red solid line is the exponential fitting using Equation 1; the red dashed line is the asymptotic value of the fit. Amplitude is shown by the orange segment. It is the difference between the fitted Φ at 2 GV and the asymptotic value C. Also indicated by the dotted green line is the Maximum Affected Rigidity R_M. Above R_M, a constant fit yields better χ^2 than the exponential fit. Adapted from Wang et al. (2023).

where Φ_{norm} is the normalized cosmic ray flux (with respect to pre-event flux) measured at the day when the FD reaches its minimum, R is the rigidity, and C is the asymptotic value of Φ_{norm} as $R \to \infty$. The amplitude A is the difference between the fitted Φ at 2 GV and the asymptotic value C. This is illustrated by the orange line segment in the cartoon shown in Figure 1. Besides the amplitude A, Wang et al. (2023) also identified the Maximum Affected Rigidity R_M, which is the rigidity up to which the effects of Forbush decreases (FDs) on Galactic Cosmic Rays (GCRs) are still significant. We do not consider the effect of R_M on the GEC in this work.

In Wang et al. (2023), FDs of two different types are considered. The first type of FD is caused by Interplanetary Coronal Mass Ejections (ICMEs) and the second is caused by Corotating Interaction Regions (CIRs). Wang et al. (2023) found that the FD amplitude of ICME FDs has a moderate correlation with the minimum Dst index and several solar wind parameters, such as maximum temperature, pressure, and magnetic field. However, for CIR FD events, neither the FD amplitude nor the Maximum Affected Rigidity showed a significant correlation with solar wind parameters. As can be seen in Table 1, in our study only three events are CIR events. Furthermore, only one of them has $A \geq 10\%$. Since FD caused by ICMEs also correlate with the Dst index, we therefore also examine the correlation between PG and the Dst index (and the Kp index).

We divide FD events into two categories. One is mild FDs with $A \leq 10\%$ and one is intense FDs with $A > 10\%$. We then analyze the PG diurnal variation, in fair weather conditions, during mild and intense FDs separately. In order to remove possible SPE effects (Tacza et al., 2018), we have limited our choice of FDs to those where SPEs did not occur one (four) day before (after) the FD onset. PG hourly values that did not meet fair weather conditions were removed.

For the analysis of the PG data, we follow closely to Tacza et al. (2018): first, monthly mean curves of the PG diurnal variation, in fair weather conditions, were calculated for each month (referred to as monthly standard curves). Next, for each FD event, a time window of 168 hr (7 days) before and after the minimum time of the event is used, where the minimum time (with time resolution of an hour) of the FD is defined as the maximum of the FD decrease observed in three Neutron Monitor stations (Oulu-Finland, Rome-Italy and Athens-Greece NM have been used). We do not use ISS/AMS-02 data to identify the minimum time because ISS/AMS-02 data is of 24 hr resolution. Next, in every time window, the differences between the PG hourly values and their monthly standard curves were calculated to get the PG excesses, that is, the calculated deviation of the PG from the mean value, further referred to in the text as PG deviation. Finally, the superposed epoch analysis (SEA) is applied to the PG deviation with time zero chosen as the minimum time. We remark that the choice of a threshold of $A = 10\%$ is to have roughly equal number of events in each group. It is therefore somewhat arbitrary. In subsequent work, when the sample size is larger, we will test how changing the threshold value can affect the result. This will be done in a similar way as in Ding et al. (2014). Such a study can help us to identify the best value of A above which FDs can sensitively affect the GEC system.

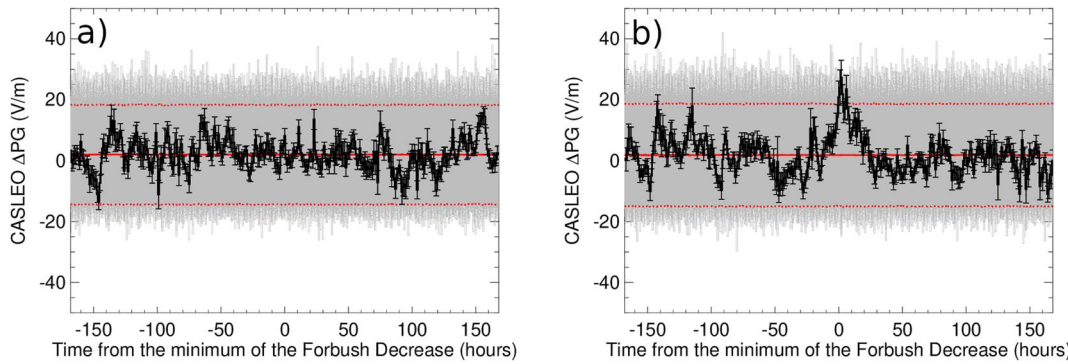

Figure 2. Superposed epoch analysis of the Potential Gradient (PG) deviation response to Forbush Decreases. The gray lines show the result of 30,000 iterations (with different time zero) of the SEA for the 10 FD events with $A \leq 10\%$ in panel (a) and 10 FD events with $A > 10\%$ in panel (b). The solid red line is the average of the iterations and the dashed red lines represent $\pm 3\sigma$ (σ is the standard deviation).

3. Results

In this section we present the behavior of the PG recorded at CASLEO (PG CASLEO), during Forbush Decreases (FD). Figure 2a shows the result of the superposed epoch analysis applied to the PG CASLEO deviations (black line) during ten (10) FDs with $A \leq 10\%$. The time zero is chosen at the minimum of the FD. The error bars represent one standard error of the mean. Each gray line is the result of the superposed epoch analysis choosing a random minimum time for the 10 FDs (30,000 iterations). The solid red line is the average of the iterations, and the dashed red lines are $\pm 3\sigma$ (σ is the standard deviation) of the average (a 99.6% confidence level). No significant PG deviation is found between $t = -150$ and $t = +150$ hr (if there is a cause-effect relationship, we are interested in period for $t > 0$). In comparison, Figure 2b presents the results of the epoch analysis for FD events with $A > 10\%$ (10 events). A clear increase of ~25 V/m in the PG (lasting ~5 hr) is observed after the FD minimum. The peak of ΔPG is roughly at $t = 2$ hr. Of these 10 events, three are large FDs, showing strong NM decreases on the Earth's surface. These are the 2015.06.22, 2012.07.14, and 2017.07.16 events in Table 1. Their percentage decreases, given by the MagnM parameter, provided by the IZMIRAN NM database, are 9.1% (1st), 7.6% (2nd), and 5.8% (5th) respectively. Their amplitude A determined from AMS-02 measurements are 15.2% (4th), 19.4% (1st), and 14.2% (5th) respectively. These events were analyzed individually by Tacza et al. (2022) and showed a significant PG increase during the FD. To see if these three events dominate the SEA analysis, we also remove these three events from our analysis to evaluate its impact on our results. This is shown in Figure 3 where the black solid line represents the epoch analysis for all 10 events and the blue solid line for the seven events without including these three. Note that the X axis is ±2 days from the zero time. The increase of PG around $t \sim 1$ hr is still significant at the $\pm 3\sigma$ level but lasting shorter (only 1 hr).

If the FDs do affect the measured PG, it must be through the change of the ionization of the atmosphere. If the atmosphere ionization profile responded to FDs right away when FDs start, one might expect that there could also be signal of a ΔPG when the time zero is chosen as the start time of FDs. This is shown in Figure 4. Panel (a) of Figure 4 shows the result of the SEA applied to the PG CASLEO deviations (black line) during the ten (10) FDs with $A \leq 10\%$. Again, the error bars represent one standard error of the mean. Each gray line is the result of the superposed epoch analysis choosing random minimum times for the 10 FDs (30,000 iterations). The solid red line is the average of the iterations, and the dashed red lines are $\pm 3\sigma$ (σ is the standard deviation) of the average (99.6% confidence level). No significant PG deviation is found after the zero time. In the same way, Figure 4b presents the results of the epoch analysis for FD events where $A > 10\%$ (10 events). We find no significant PG deviation at the 3σ value. However, at 2.5σ level, we can see that at about $t = 25$ hr, there is a peak of ΔPG. Since the FD minimum often occurs about 1 day from the FD onset, this peak is the manifestation of the peak occurred in Figure 2b. Comparing Figures 2b and 4b, we see clearly that the FD minimum time is a better indicator than the FD onset of PG variation.

Since Wang et al. (2023) found that the FD amplitude of ICME FDs has a moderate correlation with the minimum Dst index and certain solar wind parameters, and since most of the events in our study are ICME FDs (see Table 1), we now examine the correlation between PG and the Dst and Kp indices.

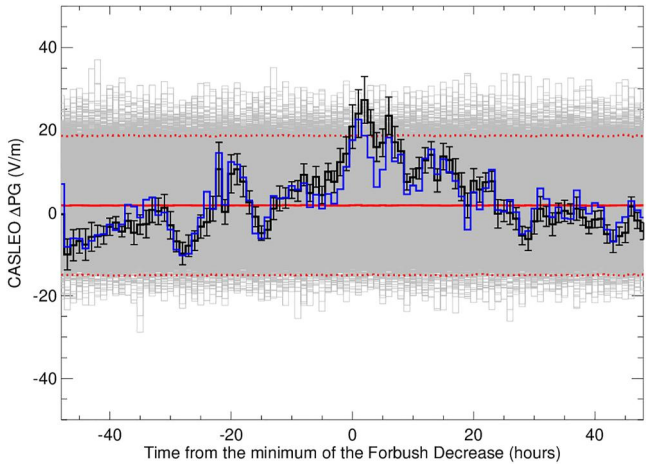

Figure 3. Similar to Figure 2b but with the blue line indicating the epoch analysis without the three strongest FDs examined in Tacza et al. (2022). See text for details.

Figures 5 and 6 show the SEA for different geomagnetic parameters for the FD events with $A \leq 10\%$ and $A > 10\%$, respectively. The zero time indicate the maximum decrease of the galactic cosmic ray flux. The temporal variation of the interplanetary magnetic field (IMF) and the z-component of the magnetic field are shown in the top panel (black and red curves, respectively). The second panel shows the solar wind plasma speed (km/s). The third panel shows the Dst and Kp indexes (black and red curves, respectively). The fourth panel show the neutron monitor counts, in percentage, for three different stations (Oulu, Rome, and Athens). The last panel shows the PG CASLEO deviation (black curve). This the same as shown in Figures 2a and 2b. The error bars in all panels show the standard errors from the 10 events in the SEA. For FD events with $A \leq 10\%$ (Figure 5), the IMF has a value of ∼10 nT around the zero time, the Bz reaches a value of ∼4 nT some hours before the zero time and drops to ∼−2 nT 12 hr after. The solar wind speed maintains a plateau for a 2-day period (from 1 day before to 1 day after time zero) at ∼480 km/s. The Dst (Kp) index reach its minimum (maximum) value of ∼−35 nT (∼3) 18 hr after time zero. The NM data for all three stations reach their minimum at time zero. The rigidity of these three NMs are 0.81 GV (Oulu), 6.27 GV (Rome), and 8.53 GV (Athens). Finally, the PG deviation is shown in the 5th panel. The PG deviation does not show any significant variation near time zero, nor is there any correlation between PG deviation and Dst/Kp indices (or solar wind parameters). For FD events $A > 10\%$ (Figure 6), the IMF has a value around ∼19 nT at time zero. Bz has ∼4 nT 1 day before time zero, then the values start to decrease reaching a minimum of ∼−7 nT ∼ 6 hr before time zero. For the solar wind, it is interesting to note that the value starts to decrease 5 days before $t = 0$ and reaches a minimum (340 km/s) 2 days before time zero. It then increases reaching a maximum value (550 km/s) at time zero. The Dst (Kp) index reaches its minimum (maximum) of −95 nT (5) at time zero. For NM data, the Oulu NM reaches its minimum (a 3% decrease) at time zero, but the Athens NM reaches its minimum (a 2% decrease) 1 day after time zero. The Rome data shows a clear decrease at time zero, but has a rather plateau-like minimum between $t = 0$ and $t = 2$ days. The difference among different NMs could be due to their different rigidities. We note that there is clear daily variations of the NM data in all three NMs. The daily variation in GCR flux detected by NMs is primarily caused by local anisotropy due to the diffusion of GCRs (largely along the interplanetary magnetic field) and the solar wind convection. Additionally, the asymmetry of the Earth's magnetosphere and the day-night difference in atmospheric structure contribute to this diurnal variation (Oh et al., 2010). Finally, the PG deviation is shown in the 5th panel. The increase of ∼28 V/m at $t \sim 2$ hr correlates very well with the dip (peak) of the Dst (Kp) index.

Perhaps the most important result of this work is the finding that there is significant increase of PG during FD events that have $A > 10\%$, but not for FD events that have $A \leq 10\%$. Furthermore, for FD events with $A > 10\%$,

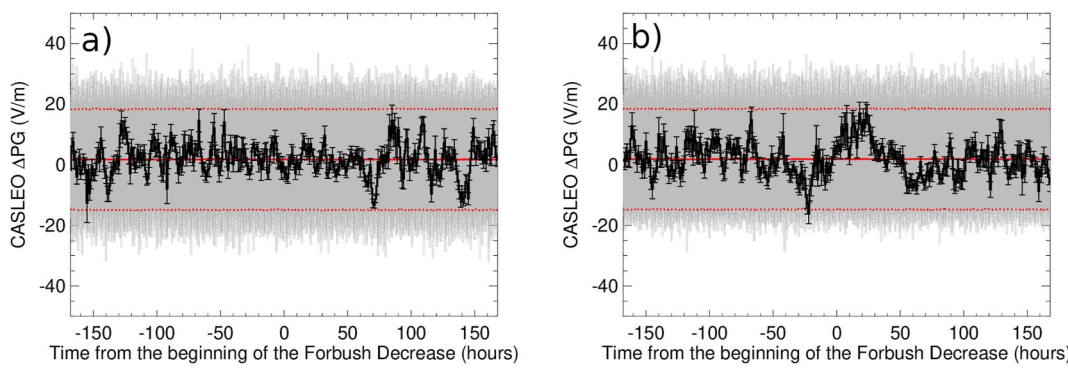

Figure 4. SEA of the PG deviation in response to FDs. Similar to Figure 2 but with the time zero for the SEA chosen to be the start of the FDs. Panel (a) is for the 10 events with $A \leq 10\%$ and Panel (b) is for the 10 events with $A > 10\%$. In both panels, the gray lines show the result of 30,000 iterations doing the average of the at different times. The solid red line is the average of the iterations and the dashed red lines represent $\pm 3\sigma$ (σ is the standard deviation).

10.1029/2023SW003852

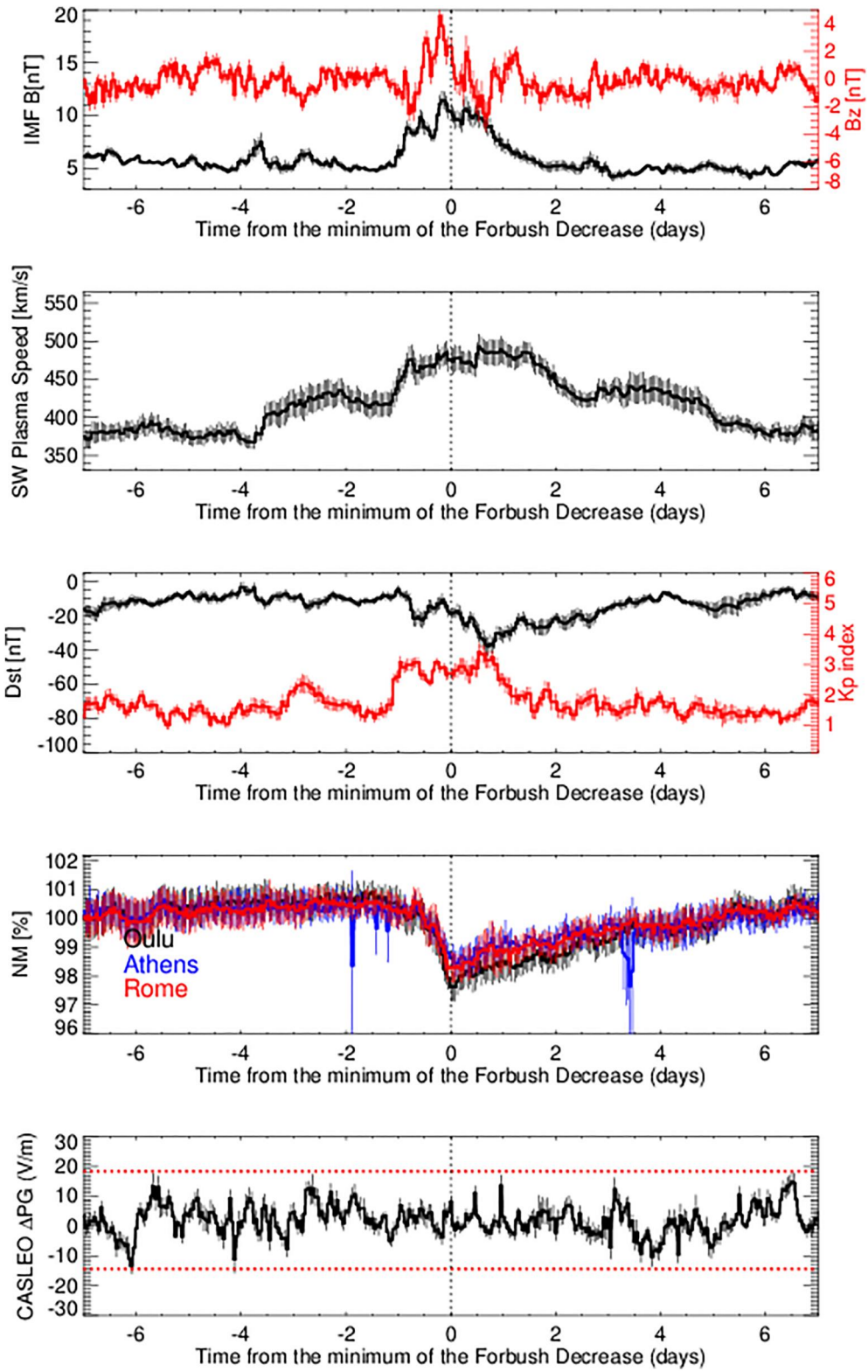

Figure 5. SEA of various solar wind parameters and the Dst/Kp indices for FD events with $A \leq 10\%$. From top to bottom these panels are: the temporal variation of the interplanetary magnetic field (IMF), the z-component magnetic field (Bz), the solar wind plasma speed, the Dst and Kp indices, the neutron monitor data, and the CASLEO PG data. The panel of the CASLEO data is the same as shown in Figure 2a. In all panels, the vertical dotted line indicates time zero.

10.1029/2023SW003852

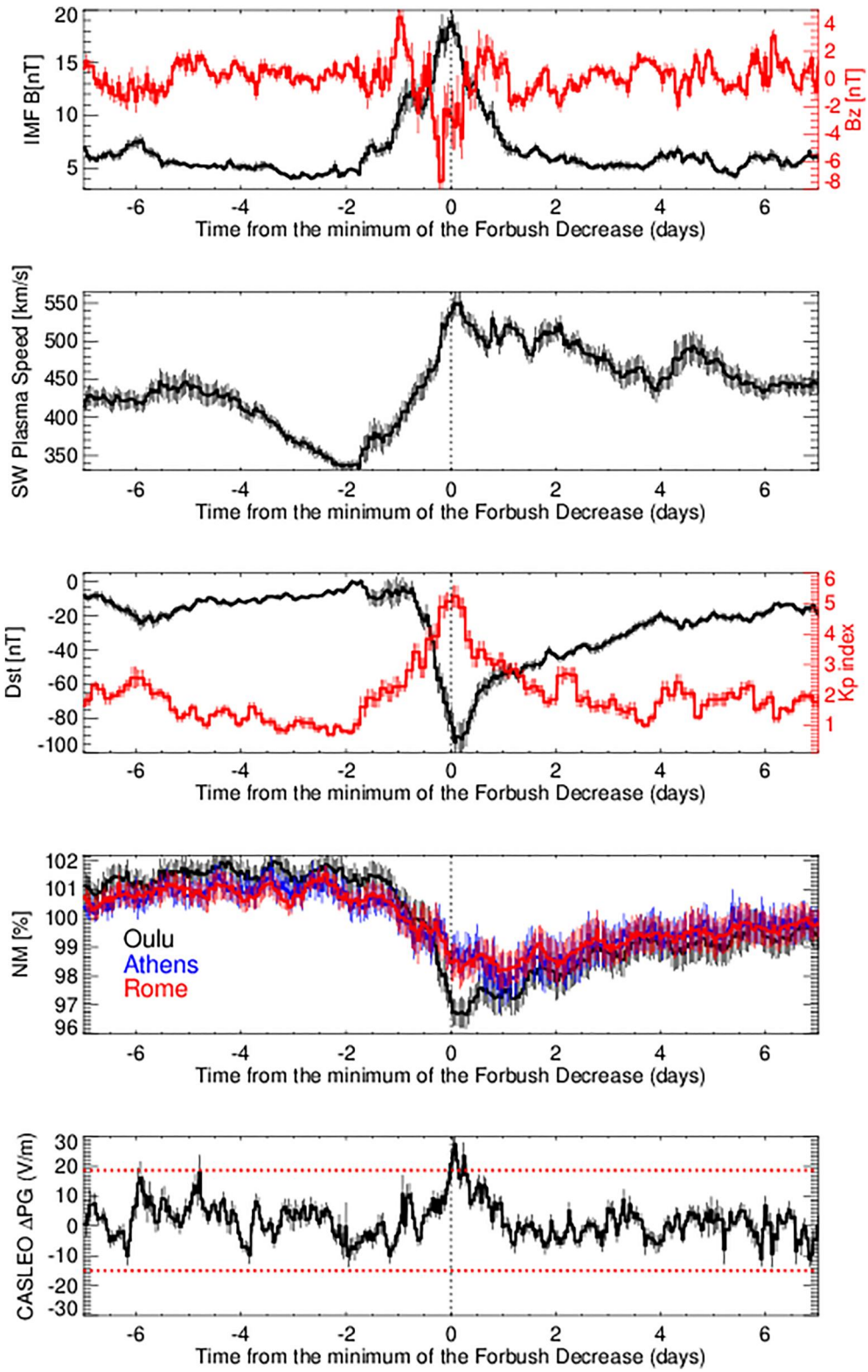

Figure 6. Same as Figure 5 but for events with $A > 10\%$. The panel of the CASLEO data is the same as shown in Figure 2b.

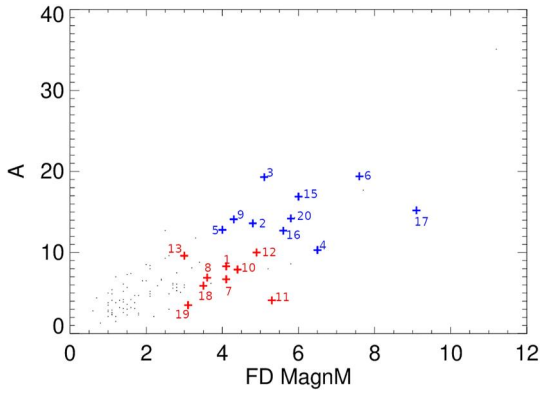

Figure 7. The scatter plot of A and the IZMIRAN MagnM values of the FD events reported in Wang et al. (2023). The small black dots are events without PG data; blue "+" are events with $A > 10\%$; and red "+" are events with $A \leq 10\%$. Event numbers are labeled next to the symbols.

there appears to be a clear change of Dst/Kp at time zero, which correlates with the increase of PG shortly after time zero (~2 hr), but not for events with $A \leq 10\%$. These findings are best illustrated in Figures 5 and 6. Comparing Figures 5 and 6, we find that,

- First, during FD events with $A > 10\%$, the Dst and Kp indices are affected more than FD events with $A \leq 10\%$. This finding alone suggests that the amplitude parameter A from AMS-02/ISS measurement is a better parameter than the IZMIRAN MagnM parameter in signaling a change of the geomagnetic field (i.e., Dst/Kp indices). This is perhaps not too surprising since the amplitude parameter A is defined on 2 GV GCRs at an altitude of ~380 km above sea surface and the MagnM parameter is most sensitive for 10 GV GCRs at sea level. Since GCRs of higher rigidity is less affected by the geomagnetic field, so it is expected that 2 GV GCRs is more sensitive to geomagnetic field change than 10 GV GCRs. Furthermore, at an altitude of ~380 km, the AMS-02/ISS observation is closer to the boundary of Earth's magnetosphere than those NMs on the ground, therefore less affected by interaction with Earth's atmosphere; Consequently, one expects that the amplitude A measured at AMS-02/ISS is a better indicator for an increase of PG than NM observations on the ground.
- Second, for FD events with $A > 10\%$, there is strong correlation between ΔPG and the variation of Dst/Kp indices; but for FD events with $A \leq 10\%$, no such correlation exists because ΔPG shows no discernible pattern for the entire period of ±6 days from time zero. This suggests that for FDs with $A > 10\%$, the change of Earth's magnetic field, as indicated by the Dst/Kp index, may affect the penetration of GCRs into Earth's atmosphere up to a level such that the ionization of the Earth's atmosphere is significantly altered, leading to the increase of PG. The interesting thing to notice is that for $A \leq 10\%$ events, the Dst index in Figure 5, like ΔPG, does not show a clear change around time zero. The *Kp* index, however, does show an enhancement around time zero. So, it appears that for FD events with $A \leq 10\%$, while the Kp index shows some correlation with GCR decreases measured by NMs on the ground, the Dst index behaves more like the PG. This raises the question: why does the increase of PG during FD events correlate well with the Dst index? And why do the PG and Dst index only show significant changes for FD events with a large A? Future study to answer these questions should be pursued.

A practical question is why to use A to classify FD events, but not the IZMIRAN MagnM value? From Table 1, we see that in general a larger A tend to have a larger MagnM. Figure 7 is a scatter plot of the amplitude A and the MagnM value for the FD events examined in Wang et al. (2023). There is a general correlation between A and MagnM. Indeed, if we choose MagnM = 4.5% as the threshold to perform the SEA, we obtain similar results as choosing $A = 10\%$. This is shown in Figure 8. For 10 FD events with MagnM >4.5%, we find that the PG shows a peak at the 3-σ level around $t = 2$ hr; for 10 FD events with MagnM < 4.5%, PG shows no signal at or after time zero. This is as expected, since 8 out of 10 events in Figure 2a (b) and Figure 8a (b) are the same. Comparing

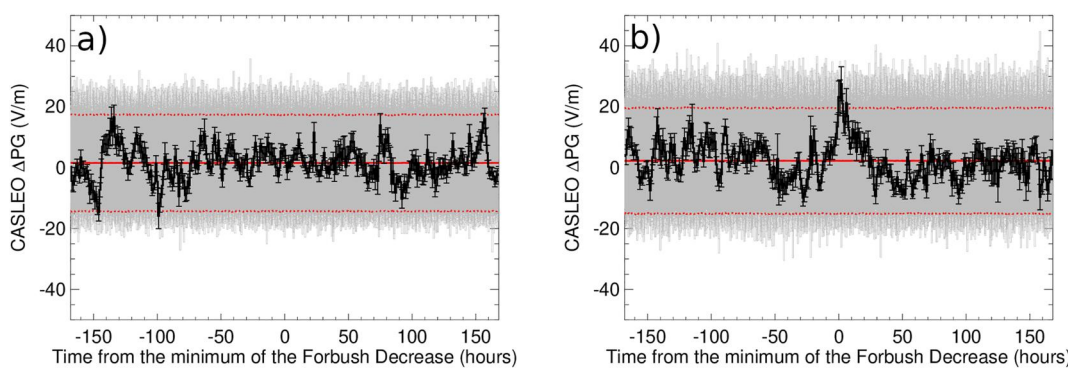

Figure 8. Similar to Figure 2, but using MagnM = 4.5% as the threshold instead of $A = 10\%$. Panel (a) is for FDs with a MagnM < 4.5% and panel (b) is for FDs with a MagnM > 4.5%.

Figures 2b and 8b, we see that events 5 and 9 in Figure 2b are replaced by events 11 and 12 in Figure 8b. This, however, did not lead to a significant difference between these two figures. We have also performed SEA of 12 events with the threshold as $A > 10\%$ or MagnM > 4.5% and the result (not shown here) is similar to Figures 2b and 8b. We expect that when more events have the A value available, a more accurate threshold could be identified. This will be pursued in a future work.

There are several reason why we choose A to classify FD in this study. First, A has a larger range than the FD MagnM value. For our events examined in this study, we have range of A from 3% to 20%. This is to be compared with the range of MagnM, from 3% to 9%. Second, as shown in Figure 7, the scatter of the correlation between A and MagnM can be large. For example, for events with MagnM between 5% and 5.5%, their A values has a large spreading from 4% to 19%. Conversely, for events with $A > 10\%$, their MagnM values vary from 4% to 9%. If we consider all events studied in Wang et al. (2023) (including the black symbols in Figure 7), this scattering is even larger, the MagnM values now range from 2.5% to 9% (excluding the one outlier with $A = 35\%$, MagnM = 11.25%). Finally, as we discussed earlier, A measures the primary GCRs at an altitude of 380 km and contains no complications involved with the generation of secondary particles. In comparison, the MagnM measures the secondary neutron at ground. To compute the MagnM value, NMs at different locations are needed. We therefore expect using A to provide a more accurate estimate of the primary GCR reduction during FD events.

A lot of efforts have been put forth to obtain the primary cosmic ray spectrum from NM count rates at the ground. Clem and Dorman (2000) used the FLUKA package to follow the transport of particles through atmosphere and determined the detection response (i.e., the response function) of different neutron monitors. Similar approaches, using the PLANETOCOSMICS GEANT-4 simulation tool, has been taken by Mishev et al. (2013, 2020). Recently Xaplanteris et al. (2021) have adopted a Quantum Field Theory approach to examine the interaction of very high energy cosmic rays with atmosphere and compute the response function. These studies are based on Monte-Carlo simulations and aim to map the NM counting rates at the ground to the primary cosmic ray spectrum. Using the Neutron Monitor Database (NMDB), one can obtain real-time updates on the change of the primary cosmic ray flux (often due to Ground Level Enhancement Events and FDs) (Mavromichalaki et al., 2011). It is conceivable that one can add an intermediate step, corresponding to the ISS location, during the Monte-Carlo simulation and obtain a mapping between NM counting rates and the GCR spectrum at the ISS (assuming there is a clear difference between ISS and L1). Comparing ISS data with this mapping can provide further insights to the interaction of cosmic rays with Earth's atmosphere. We remark that in a recent work, McJannet and Desilets (2023) compared count rates from different NMs against that from a reference NM (e.g., the Climax NM) and found that there exists one single parameter (which is location dependent) that allows one to compute any NM counts from a reference NM counts. This is validated for quiet time, but not during CMEs, which, in part could be due to configuration change of the Earth's magnetosphere during CMEs. The effect of magnetosphere on the propagation of cosmic rays are often described by a single parameter, the effective geomagnetic cutoff R_c, which depends on latitude and longitude. In computing R_c, configuration of Earth's magnetic field has to be given, which of course, can change when a geomagnetic storm occurs. Nevertheless, once the coupled system of the solar wind and Earth's magnetosphere is prescribed (Lin & Wang, 2005; Omelchenko et al., 2021), one can use Monte-Carlo simulations, for example, as in Larsen et al. (2023), to investigate the transport of cosmic rays in Earth's magnetosphere.

In our context, a study to examine and understand the relationship between A and the decrease of neutron rates by NMs around the globe would be helpful to understand the PG measured at various stations. The coupling between NM counting rate and the primary cosmic ray spectrum requires the knowledge of the Earth's atmosphere density and its composition, etc., which can be uniquely identified by, for example, Planet Specification File (PSF). With this knowledge, one can in principle compute the atmosphere ionization profile at any particular location. Such a practice has been earlier exercised by Usoskin et al. (2010), and more recently by Winant et al. (2023). Using a GEANT-4-based Atmospheric Radiation Interaction Simulator (AtRIS) toolkit (Banjac et al., 2019), Winant et al. (2023) examined ionization profiles at multiple locations for an extended period in 2014, focusing on clear seasonal effect. Such a calculation during specific FDs would be necessary to interpret the PG observations. This will be pursued in a future work.

4. Conclusions

Solar Energetic Particle events (SEPs) and Forbush Decreases of GCRs are two important Space Weather events. Over the past decades, they have been speculated to be also able to affect the global electric circuit (GEC), and through which, affecting the weather patterns such as thunderstorms and lightnings on the Earth. Tacza et al. (2022) performed SEA on 17 large SEP events and showed that at the 2.5σ level, there is a correlation between SEP flux increase and PG increase at fair weather conditions. Less clear is the effect of FDs on PG. Previous studies seem to have reached different conclusions. The work of Tacza et al. (2022) examined three individual large FD events and showed that PGs in all three events increase shortly after the FDs reach their maximum GCR reduction.

In this work, we extend (Tacza et al., 2022) and perform a statistical study to examine the correlation between PG variations and Forbush Decreases. Unlike previous work where FDs are classified by ground Neutron Monitor data, we classify FD events using primary GCR measurements obtained by the Alpha Magnetic Spectrometer (AMS-02) onboard the International Space Station. Specifically, we use amplitude A defined in Wang et al. (2023), instead of the often used parameter MagnM, to classify FD events. Comparing to NMs which obtained secondary neutrons with a coarse energy resolution at the ground, the AMS-02 measurements directly measure the primary cosmic rays at a higher altitude with a much finer energy resolution. Consequently, it offer better energy resolution and lower systematic uncertainties and may help us to reveal more precisely the causality relationship between FD and increase of PG. For PG data, we use that recorded at CASLEO (low latitude, 2550 m a.s.l.) during fair weather conditions. A total of 20 events were identified which have both AMS-02 GCR measurement and PG fair weather measurement. In order to enhance some possible weak effects, we applied the SEA method and remove the noise produced by meteorological parameters. We find that for FD events with $A > 10\%$, there is significant increases of PG shortly (~2 hr) when FD reaches its maximum reduction, but not for FD events that have $A \leq 10\%$, as shown in Figure 2. Furthermore, for FD events with $A > 10\%$, there appears to be a clear change of Dst/Kp at time zero, which correlates with the increase of PG shortly after time zero (~2 hr), but not for events with $A \leq 10\%$, as shown in Figures 5 and 6. We note that FDs with large MagnM often have large A, and vice versa. However, the scattering can be large, as shown in Figure 7. Because the range of the A is larger than the range of MagnM, it is desirable to use A as the variable when examining the PG variations. Our findings suggest that large FDs ($A > 10\%$) can significantly affect the GEC, leading to an increase of PG after the FDs reach their maximum. This effect is closely related to the change of the Earth's magnetosphere configuration since the Dst/Kp indices also show significant changes. In future works, we will examine PGs from other stations to examine if the PG variation show clear latitude and altitude dependence. We will also examine how the threshold of A can affect the conclusion.

Data Availability Statement

Solar and geomagnetic indexes (IMF, Bz, solar wind speed, Dst, and Kp indexes) are publicly available from https://omniweb.gsfc.nasa.gov/form/dx1.html. Neutron monitor data are publicly available from https://www.nmdb.eu/nest/. Original data for all events and plots presented in the paper are archived in a dataset (Tacza et al., 2024).

Acknowledgments
This work is supported in part by NSF-SHINE Grant 2301365 and NSF-ANSWERS Grant 2149771 at UAH. Supports by ISSI and ISSI-BJ through the international team 581 is also acknowledged. JPR thanks CNPq (project 311927/2022-0) and CAPES (project 88881.310386/2018-01).

References

Alania, M. V., & Wawrzynczak, A. (2008). Forbush decrease of the galactic cosmic ray intensity: Experimental study and theoretical modeling. *Astrophysics and Space Sciences Transactions*, *4*(2), 59–63. https://doi.org/10.5194/astra-4-59-2008

Alania, M. V., & Wawrzynczak, A. (2012). Energy dependence of the rigidity spectrum of Forbush decrease of galactic cosmic ray intensity. *Advances in Space Research*, *50*(6), 725–730. https://doi.org/10.1016/j.asr.2011.09.027

Banjac, S., Herbst, K., & Heber, B. (2019). The atmospheric radiation interaction simulator (AtRIS): Description and validation. *Journal of Geophysical Research: Space Physics*, *124*(1), 50–67. https://doi.org/10.1029/2018JA026042

Belov, A., Baisultanova, L., Eroshenko, E., Mavromichalaki, H., Yanke, V., Pchelkin, V., et al. (2005). Magnetospheric effects in cosmic rays during the unique magnetic storm on November 2003. *Journal of Geophysical Research*, *110*(A9), A09S20. https://doi.org/10.1029/2005JA011067

Belov, A., Eroshenko, E., Yanke, V., Oleneva, V., Abunin, A., Abunina, M., et al. (2018). The global survey method applied to ground-level cosmic ray measurements. *Solar Physics*, *293*(4), 68. https://doi.org/10.1007/s11207-018-1277-6

Cane, H. V. (2000). Coronal mass ejections and Forbush decreases. *Space Science Reviews*, *93*(1/2), 55–77. https://doi.org/10.1023/A:1026532125747

Chree, C. (1913). III. Some phenomena of sunspots and of terrestrial magnetism at Kew Observatory. *Philosophical Transactions of the Royal Society of London - Series A: Containing Papers of a Mathematical or Physical Character*, *212*(484–496), 75–116. https://doi.org/10.1098/rsta.1913.0003

Clem, J. M., & Dorman, L. I. (2000). Neutron monitor response functions. *Space Science Reviews*, *93*(1/2), 335–359. https://doi.org/10.1023/A:1026508915269

Ding, L. G., Li, G., Dong, L. H., Jiang, Y., Jian, Y., & Gu, B. (2014). On the identification of time interval threshold in the twin-CME scenario. *Journal of Geophysical Research: Space Physics*, *119*(3), 1463–1475. https://doi.org/10.1002/2013JA019745

Dorman, L. (2004). *Cosmic rays in the Earth's atmosphere and underground*. Springer. https://doi.org/10.1007/978-1-4020-2113-8

Engfer, D. W., & Tinsley, B. A. (1999). An investigation of short-term solar wind modulation of atmospheric electricity at Mauna Loa Observatory. *Journal of Atmospheric and Solar-Terrestrial Physics*, *61*(13), 943–953. https://doi.org/10.1016/S1364-6826(99)00057-7

Guo, X., & Florinski, V. (2014). Galactic cosmic-ray modulation near the heliopause. *The Astrophysical Journal*, *793*(1), 18. https://doi.org/10.1088/0004-637X/793/1/18

Haldoupis, C., Rycroft, M., Williams, E., & Price, C. (2017). Is the "Earth-ionosphere capacitor" a valid component in the atmospheric global electric circuit? *Journal of Atmospheric and Solar-Terrestrial Physics*, *164*, 127–131. https://doi.org/10.1016/j.jastp.2017.08.012

Harrison, R. (2013). The Carnegie curve. *Surveys in Geophysics*, *34*(2), 209–232. https://doi.org/10.1007/s10712-012-9210-2

Harrison, R., & Nicoll, K. (2018). Fair weather criteria for atmospheric electricity measurements. *Journal of Atmospheric and Solar-Terrestrial Physics*, *179*, 239–250. https://doi.org/10.1016/j.jastp.2018.07.008

Larsen, N., Mishev, A., & Usoskin, I. (2023). A new open-source geomagnetosphere propagation tool (OTSO) and its applications. *Journal of Geophysical Research: Space Physics*, *128*(3), e2022JA031061. https://doi.org/10.1029/2022JA031061

Lin, Y., & Wang, X. Y. (2005). Three-dimensional global hybrid simulation of dayside dynamics associated with the quasi-parallel bow shock. *Journal of Geophysical Research*, *110*(A12), A12216. https://doi.org/10.1029/2005JA011243

Liu, C., Williams, E. R., Zipser, E. J., & Burns, G. (2010). Diurnal variations of global thunderstorms and electrified shower clouds and their contribution to the global electrical circuit. *Journal of the Atmospheric Sciences*, *67*(2), 309–323. https://doi.org/10.1175/2009JAS3248.1

Marcz, F. (1997). Short-term changes in atmospheric electricity associated with forbush decreases. *Journal of Atmospheric and Solar-Terrestrial Physics*, *59*(9), 975–982. https://doi.org/10.1016/S1364-6826(96)00076-4

Mavromichalaki, H., Papaioannou, A., Plainaki, C., Sarlanis, C., Souvatzoglou, G., Gerontidou, M., et al. (2011). Applications and usage of the real-time neutron monitor database. *Advances in Space Research*, *47*(12), 2210–2222. https://doi.org/10.1016/j.asr.2010.02.019

McJannet, D. L., & Desilets, D. (2023). Incoming neutron flux corrections for cosmic-ray soil and snow sensors using the global neutron monitor network. *Water Resources Research*, *59*(4), e2022WR033889. https://doi.org/10.1029/2022WR033889

Mishev, A. L., Koldobskiy, S. A., Kovaltsov, G. A., Gil, A., & Usoskin, I. G. (2020). Updated neutron-monitor yield function: Bridging between in situ and ground-based cosmic ray measurements. *Journal of Geophysical Research: Space Physics*, *125*(2), e27433. https://doi.org/10.1029/2019JA027433

Mishev, A. L., Usoskin, I. G., & Kovaltsov, G. A. (2013). Neutron monitor yield function: New improved computations. *Journal of Geophysical Research: Space Physics*, *118*(6), 2783–2788. https://doi.org/10.1002/jgra.50325

Nicoll, K., Harrison, R., Barta, V., Bor, J., Brugge, R., Chillingarian, A., et al. (2019). A global atmospheric electricity monitoring network for climate and geophysical research. *Journal of Atmospheric and Solar-Terrestrial Physics*, *184*, 18–29. https://doi.org/10.1016/j.jastp.2019.01.003

Oh, S. Y., Yi, Y., & Bieber, J. (2010). Modulation cycles of galactic cosmic ray diurnal anisotropy variation. *Solar Physics*, *262*(1), 199–212. https://doi.org/10.1007/s11207-009-9504-9

Okike, O. (2019). Investigation of forbush decreases and other solar/geophysical agents associated with lightning over the U.S. latitude band and the continental Africa. *Journal of Geophysical Research: Space Physics*, *124*(6), 3910–3925. https://doi.org/10.1029/2018JA026456

Okike, O., & Umahi, A. (2019). Cosmic ray—Global lightning causality. *Journal of Atmospheric and Solar-Terrestrial Physics*, *189*, 35–43. https://doi.org/10.1016/j.jastp.2019.04.002

Omelchenko, Y. A., Roytershteyn, V., Chen, L.-J., Ng, J., & Hietala, H. (2021). HYPERS simulations of solar wind interactions with the Earth's magnetosphere and the Moon. *Journal of Atmospheric and Solar-Terrestrial Physics*, *215*, 105581. https://doi.org/10.1016/j.jastp.2021.105581

Rycroft, M., Harrison, G., Nicoll, K., & Mareev, E. (2008). An overview of Earth's global electric circuit and atmospheric conductivity. *Space Science Reviews*, *137*(1–4), 1572–9672. https://doi.org/10.1007/s11214-008-9368-6

Rycroft, M., Nicoll, K., Aplin, K., & Harrison, G. (2012). Recent advances in global electric circuit coupling between the space environment and the troposphere. *Journal of Atmospheric and Solar-Terrestrial Physics*, *90–91*, 198–211. (Recent Progress in the Vertical Coupling in the Atmosphere-Ionosphere System). https://doi.org/10.1016/j.jastp.2012.03.015

Sheftel, V., Bandilet, O., Yaroshenko, A., & Chernyshev, A. (1994). Space-time structure and reasons of global, regional, and local variations of atmospheric electricity. *Journal of Geophysical Research*, *99*(D5), 10797–10806. https://doi.org/10.1029/93JD02857

Simpson, J. A. (1954). Cosmic-radiation intensity-time variations and their origin. III. The origin of 27-day variations. *Physics Reviews*, *94*(2), 426–440. https://doi.org/10.1103/PhysRev.94.426

Tacza, J., Li, G., & Raulin, J.-P. (2024). Effects of Forbush decreases on the global electric circuit [Dataset]. *Zenodo*. https://doi.org/10.5281/zenodo.10441524

Tacza, J., Odzimek, A., Tueros Cuadros, E., Raulin, J.-P., Kubicki, M., Fernandez, G., & Marun, A. (2022). Investigating effects of solar proton events and Forbush decreases on ground-level potential gradient recorded at middle and low latitudes and different altitudes. *Space Weather*, *20*(3), e2021SW002944. https://doi.org/10.1029/2021SW002944

Tacza, J., Raulin, J.-P., Macotela, E., Marun, A., Fernandez, G., Bertoni, F., et al. (2020). Local and global effects on the diurnal variation of the atmospheric electric field in South America by comparison with the Carnegie curve. *Atmospheric Research*, *240*, 104938. https://doi.org/10.1016/j.atmosres.2020.104938

Tacza, J., Raulin, J.-P., Mendonca, R. R. S., Makhmutov, V. S., Marun, A., & Fernandez, G. (2018). Solar effects on the atmospheric electric field during 2010–2015 at low latitudes. *Journal of Geophysical Research: Atmospheres*, *123*(21), 11970–11979. https://doi.org/10.1029/2018JD029121

Tacza, J., Raulin, J.-P., Morales, C., Macotela, E., Marun, A., & Fernandez, G. (2021). Analysis of long-term potential gradient variations measured in the Argentinian Andes. *Atmospheric Research*, *248*, 105200. https://doi.org/10.1016/j.atmosres.2020.105200

Usoskin, I. G., Braun, I., Gladysheva, O. G., Hörandel, J. R., Jämsén, T., Kovaltsov, G. A., & Starodubtsev, S. A. (2008). Forbush decreases of cosmic rays: Energy dependence of the recovery phase. *Journal of Geophysical Research*, *113*(A7). https://doi.org/10.1029/2007JA012955

Usoskin, I. G., Kovaltsov, G. A., & Mironova, I. A. (2010). Cosmic ray induced ionization model CRAC: CRII: An extension to the upper atmosphere. *Journal of Geophysical Research*, *115*(D10). https://doi.org/10.1029/2009JD013142

Wang, S., Bindi, V., Consolandi, C., Corti, C., Light, C., Nikonov, N., & Kuhlman, A. (2023). Properties of Forbush decreases with AMS-02 daily proton flux data. *The Astrophysical Journal*, *950*(1), 23. https://doi.org/10.3847/1538-4357/acca1b

Wijsen, N., Li, G., Ding, Z., Lario, D., Poedts, S., Filwett, R. J., et al. (2023). On the seed population of solar energetic particles in the inner heliosphere. *Journal of Geophysical Research: Space Physics*, *128*(3), e2022JA031203. https://doi.org/10.1029/2022JA031203

Wilson, C. T. R. (1921). Investigations on lightning discharges and on the electric field of thunderstorms. *Philosophical Transactions of the Royal Society of London - Series A: Containing Papers of a Mathematical or Physical Character*, *221*, 73–115. Retrieved from http://www.jstor.org/stable/91189

Winant, A., Pierrard, V., Botek, E., & Herbst, K. (2023). The atmospheric influence on cosmic-ray-induced ionization and absorbed dose rates. *Universe*, *9*(12), 502. https://doi.org/10.3390/universe9120502

Wu, Q., Li, H., & Wang, C. (2019). Lightning response during forbush decrease in the tropics and subtropics. *Journal of Atmospheric and Solar-Terrestrial Physics*, *195*, 105134. https://doi.org/10.1016/j.jastp.2019.105134

Xaplanteris, L., Livada, M., Mavromichalaki, H., & Dorman, L. (2021). A new approximate coupling function: The case of Forbush decreases. *New Astronomy*, *82*, 101453. https://doi.org/10.1016/j.newast.2020.101453

Zhang, L., Tinsley, B., & Zhou, L. (2020). Low latitude lightning activity responses to cosmic ray forbush decreases. *Geophysical Research Letters*, *47*(4), e2020GL087024. https://doi.org/10.1029/2020GL087024